AIAA SciTech Forum
13-17 January 2014, National Harbor, Maryland
52nd Aerospace Sciences Meeting

10.2514/6.2014-0009

Wing-flapping and abdomen actuation optimization for hovering in the butterfly *Idea leuconoe*

Tyler Wilson* and Roberto Albertani†
Oregon State University, Corvallis, OR, 97331, U.S.A.

A numerical model of the Tree Nymph *Idea leuconoe* was developed to determine the effects of different motion parameters on the longitudinal stability of flight. Thirteen independent motion parameters were used as inputs to describe the motion of the wings and abdomen. The model would then solve for the position and pitch history over the duration of a flight and output all relevant forces and moments. Two optimizations were performed using a genetic algorithm code, one with a fixed abdomen and another with active abdomen actuation. The goal was to find parameters that allowed the butterfly to maintain a fixed position and pitch. Results from the the optimized parameter sets were compared with a randomly generated parameter set. Experimental data from recordings of real butterflies is also presented.

I. Introduction

The biomechanics of flapping flight, and flying animals, is an area of research that has rapidly grown in the past few decades. Flapping fliers, including birds, bats, and insects, are capable of extreme unsteady maneuvers that allow them to rapidly change speed and direction, fly in confined spaces, and endure turbulent wind conditions. There are many applications to small air vehicles, where similar abilities are desired, where bio-inspiration from flapping flight could be introduced. A large amount of experimental research has been done observing flapping flights in order to determine the flight kinematics of various flappers, including bats,[1] birds,[2] and insects.[3] Most of this research focuses mainly on wingbeat kinematics, as the motion of the wings dictates the aerodynamic forces generated, which is the main factor in propulsion and maneuvering.

(a)

Figure 1. Frame from a recorded flight of a Tree Nymph butterfly. Note the angle of the abdomen with respect to the wings and body.

In observed flights of the Tree Nymph *Idea leuconoe*, shown in Figure 1, and other butterfly species, there is a large amount of abdomen motion that can be observed during flight. As the abdomen constitutes roughly 40% of the butterfly's mass, it is potentially capable of generating relevant inertial forces and moments. Live flight data has shown significant correlation between the abdomen motion and wing flapping motion in the

*Graduate Research Assistant, Mechanical, Industrial and Manufacturing Engineering, 204 Rogers Hall, AIAA Student Member.
†Associate Professor, Mechanical, Industrial and Manufacturing Engineering, 204 Rogers Hall, AIAA Member.

Tree Nymph *Idea leuconoe*,[4] indicating that the abdomen motion may indeed play a part in the butterflies' flight. This paper aims to further investigate the dynamics of the Tree Nymph *Idea leuconoe*, and specifically examine the role that the abdomen motion plays in the stability of its flight during hovering.

II. Model & Methodologies

This section details the computational model used to simulate the butterfly. The model uses motion parameter inputs to calculate the positions and orientations of the body parts, and their derivatives, at each timestep. Using the positions, velocities, and accelerations of the body parts, the instantaneous forces and moments acting on them can be calculated, which can be used to find the instantaneous acceleration and rotational acceleration. A differential equation is set that can be solved to calculate the position and orientation of the body with respect to time.

A. Numerical Model

1. Input parameters

The morphological parameters used as inputs to the model, namely the masses and dimensions of the butterfly's individual body parts, were acquired from data taken at the McGuire Center for Lepidoptera and Biodiversity in Gainesville, FL. Mass measurements were taken from dead butterflies that had recently died from natural causes. Dimension measurements were estimated from the digitized butterfly, obtained from live measurements, illustrated in Figure 2. Table 1 below lists the masses and dimensions used by the model.

Table 1. Masses and dimensions of butterfly body parts.

Thorax			Abdomen			Head		Wings		
m(g)	L(mm)	r(mm)	m(g)	L(mm)	r(mm)	m(g)	r(mm)	m(g)	L(mm)	MAC(mm)*
0.1808	10.0	6.00	0.2404	28.9	6.00	0.02	6.00	0.0578	66.1	61.0

* Mean Aerodynamic Chord

Points were acquired along the edges of the digitized wings to build a matrix of coordinates that was used to reconstruct the wings' geometry. An equivalent wing was created that merged the forewing and hindwing into a single wing with the same chord distribution as the two separate wings. Though research has shown that forewing-hindwing interactions have an effect on aerodynamic forces,[5] the difference is small(less than 5%) in hovering when the wings flap in phase. Butterflies also slightly overlap their wings when flying, which justifies combining them to act as a single wing. Density was assumed constant throughout the body parts, and the butterfly was considered bilaterally symmetric.

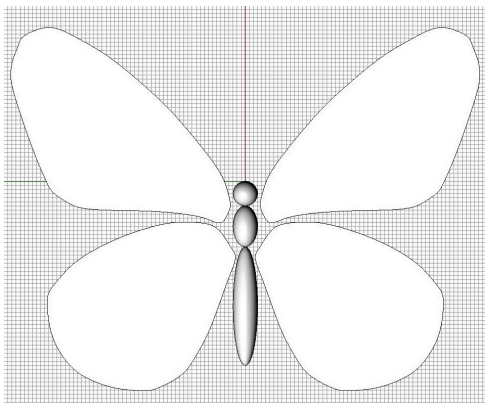

Figure 2. Digitized butterfly image with 1mm grid spacing.

2. *Coordinate System and orientation of body parts*

Two right-handed coordinate systems were used in the model - a moving body coordinate system and a fixed global coordinate system, both shown in Figure 3(d), with +Y being to the left in both coordinate systems, as seen in Figure 3(a) and (b). Each angle had its amplitude, mean, and phase individually specified, with a single frequency parameter used for all angles, totalling 13 motion parameters. The three angles defining the position of the wings were the flapping angle, sweeping angle, and feathering angle, illustrated in Figure 3, along with the abdomen angle, defined as the abdomen orientation with respect to the thorax in the symmetry plane.

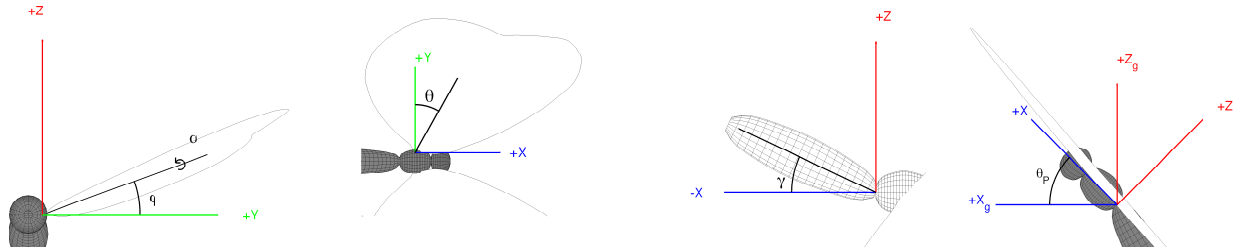

(a) (b) (c) (d)

Figure 3. (a) Flapping angle φ and feathering angle α. (b) Sweeping angle θ. (c) Abdomen angle γ. (d) Pitching angle θ_P. Note that for the wing angle figures (a) and (b), the coordinate system origin was shown at the wing root as the angles are defined from that point, though the origin of the body coordinate system is located at the abdomen root. The XYZ coordinate system is the body coordinate system, whereas the $X_gY_gZ_g$ coordinate system in (d) is the fixed global coordinate system

The value of any of the four angles at a given time t can be calculated using the following equation:

$$\theta_t = \theta_A \sin(2\pi f + \theta_p) + \theta_m \tag{1}$$

Where θ_A is the amplitude of the angle, θ_p is the phase angle, θ_m is the mean angle, and f is the frequency. The above equation can be used to calculate the angles as any time t, and subsequently the position and orientation of the wings and abdomen in the body frame at each timestep. The wing, which starts in the horizontal plane with the leading edge facing forwards, is rotated by the sweeping angle about the z-axis, then by the flapping angle about the x-axis, and finally the wing is then rotated about the wing axis by the feathering angle. The same process is applied using the angular velocity and acceleration derivatives of the angles, to determine the velocity and acceleration of the wings and abdomen, which are used in the calculation of the aerodynamic and inertial forces.

3. *Aerodynamic forces*

Aerodynamic forces were calculated using a quasi-steady state blade-element model, using 20 elements per wing. The model, using experimentally derived coefficients, accounts for forces due to wing translation, wing rotation, and inertia effects, including the added mass. The magnitude of translational force was calculated using the following equation:

$$F_t = \frac{1}{2}\rho R\bar{c}\int_0^1 C_t(\hat{r})U^2(\hat{r})\hat{r}\hat{c}(\hat{r})d\hat{r} \tag{2}$$

Where ρ is the fluid density, R is the wing radius, $\bar{c}$ is the average chord length, C_t is the translational force coefficient, U is the instantaneous velocity of the wing in the chord plane, $\hat{r}$ is the nondimensional radial position, and $\hat{c}$ is the nondimensional chord length. The translational force coefficient was calculated using the following equation:

$$\begin{aligned} C_t = \{&[1.5\sin(2\alpha - 0.06) + 0.3\cos(\alpha - 0.49) + 0.01]^2 + \\ &[1.5\sin(2\alpha - 0.06) + 0.3\cos(\alpha - 0.49) + 0.01]^2\}^{0.5} \end{aligned} \tag{3}$$

Where α is the angle of attack of the element with respect to the flow velocity in the chord plane. This equation was derived from lift and drag polars from model flapping wings of low to medium(150-8000) Reynolds numbers.[6–9] The magnitude of rotational force for each element was calculated as follows:

$$F_r = C_{rot}\rho U_t \dot{\alpha}\bar{c}^2 R \int_0^1 \hat{r}\hat{c}^2(\hat{r})d\hat{r} \tag{4}$$

Where C_{rot} is the rotational force coefficient, assumed to be 1.55, U_t is the wingtip velocity, and $\dot{\alpha}$ is the wing axis rotational velocity.[10] The force of inertia due to the added mass of the fluid was calculated as:

$$\begin{aligned} F_a = \frac{\rho\pi\bar{c}^2R^2}{4}(\ddot{\phi}\sin\alpha + \dot{\phi}\dot{\alpha}\cos\alpha)\int_0^1 \hat{r}\hat{c}^2(\hat{r})d\hat{r} \\ +\ddot{\alpha}\rho\frac{\pi}{16}\bar{c}^3R\int_0^1 \hat{c}^2(\hat{r})d\hat{r} \end{aligned} \tag{5}$$

Where $\dot{\phi}$ and $\ddot{\phi}$ are the total angular velocity and acceleration of the wing.

The three force magnitudes were summed to find the total force magnitude for each element. The force vector was assumed to act normal to the wing element surface, at a point 25% of the chord length behind the leading edge of the wing element.[11] Drag on the body parts was calculated by modelling the thorax and abdomen as cylindrical elements, with the drag on each element being calculated as:

$$D = \frac{1}{2}\rho U^2 C_d A \tag{6}$$

Where U is the velocity in the plane perpendicular to the body axis, C_d is the drag coefficient for cylinders at low Reynolds numbers(100-1000),[12] assumed to be 2, and A is the frontal area of the element.

4. Inertial and gravity forces

Inertial forces and moments due to the acceleration of the wings and abdomen with respect to the body(thorax) were calculated as follows:

$$F_I = ma_{cm} \tag{7}$$

$$M_I = I\ddot{\phi} \tag{8}$$

Where m is the mass of the body part, a_{cm} is the linear acceleration of the body part at its center of mass, I is the moment of inertia of the body part, and $\ddot{\phi}$ is the angular acceleration of the body part.

5. Center of mass and sum of forces and moments

The instantaneous center of mass of the butterfly was calculated as:

$$CoM = \frac{1}{\sum m_i}\sum m_i r_i \tag{9}$$

Where m_i are the masses of the individual body parts and r_i are the radial vectors from the origin of the body system to the center of mass of those body parts.

The instantaneous total force acting on the butterfly is the sum of the aerodynamic(wings and body) forces, inertial forces, and gravity:

$$F_{tot} = F_{aero} + F_{iner} + F_{grav} \tag{10}$$

The instantaneous total moment on the butterfly is calculated by summing the aerodynamic moments, inertial moments, and gravity moments:

$$M_i = r_i \times F_i \tag{11}$$

$$M_{tot} = M_{aero} + M_{iner} + M_{grav} \tag{12}$$

6. Solving the differential equation

The instantaneous forces and moments were used to solve for the translational and rotational accelerations, which were used with the equations of motion to form a set of ordinary differential equations:

$$\frac{\partial \vec{u}}{\partial t} = \dot{\vec{u}} \tag{13}$$

$$\frac{\partial \dot{\vec{u}}}{\partial t} = \ddot{\vec{u}} = \frac{F_{tot}}{m} \tag{14}$$

$$\frac{\partial \theta}{\partial t} = \dot{\theta} \tag{15}$$

$$\frac{\partial \dot{\theta}}{\partial t} = \ddot{\theta} = \frac{M_{tot}}{I} \tag{16}$$

Where $\vec{u}$ is the position vector and θ is the body orientation, both in the global coordinate system. Using an ODE solver, the time history of the body position and orientation, and their derivatives, can be solved for a specified flight time.

B. Parameter Optimization Scheme

To achieve hovering flight with acceptable pitch stability, the model was coupled to a genetic algorithm code to optimize the flight input parameters. The genetic algorithm used 40 individuals per generation. The reproduction parameters used were a 5% mutation probability, a 90% crossover probability, and a 10% elitism. Each optimization was allowed to run for 70 generations.

Stable hovering flight implies that a fixed position and orientation is maintained throughout the flight. Therefore, it was the goal of the genetic algorithm to minimize both the total displacement and the change in pitch orientation. A weighted sum objective function was used to combine these two objectives into one objective value that could be used to evaluate the fitness of each individual flight. The following objective function was used:

$$f_{obj} = W\Delta_\theta + (1 - W)\Delta_\chi \tag{17}$$

Where f_{obj} is the objective function value, W is the weighing factor, Δ_θ is the pitch deviation, and Δ_χ is the position deviation. The pitch and position deviation were defined as follows:

$$\Delta_\theta = \frac{1}{t}\int_0^{t_f} \frac{\theta_t - \theta_{obj}}{\theta_{norm}} \tag{18}$$

$$\Delta_\chi = \frac{1}{t}\int_0^{t_f} \frac{\chi_t - \chi_{obj}}{\chi_{norm}} \tag{19}$$

Where θ_t and χ_t are the pitch orientation and displacement at time t, θ_{obj} and χ_{obj} are the desired pitch orientation and displacement, and θ_{norm} and χ_{norm} are the scaling factors used to normalize the two objectives. Table 2 shows the desired values and scaling factors chosen for use in all optimizations:

Table 2. Objective function parameters.

W	θ_{obj} (°)	χ_{obj} (cm)	θ_{norm} (°)	χ_{norm} (cm)
0.65	30	0	360	10

Flights were optimized over 10 flaps. The initial position and pitch were set to the desired values(θ_{obj} and χ_{obj}), with their initial velocities set to zero. The bounds for all parameters were estimated based on observed flight data of real butterflies.[13]

C. Experimental Flight Data

This section briefly presents the experimental techniques used for collecting live flight data of Lepidoptera in the natural environment and discusses the data postprocessing techniques used to analyze the flights.[4]

1. Experimental Setup

All flight measurements were performed at the Butterfly Rainforest at the McGuire Center for Lepidoptera and Biodiversity, a 6,400 square foot screened vivarium at the Florida Natural History Museum in Gainesville, FL. The center includes over 460 species of subtropical and tropical plants and trees and supports up to 120 different species and 2,000 free-flying butterflies.

A vision-based estimation method was used to study the insects flight with negligible interference on their natural behavior. The visual system was composed of two high-speed digital cameras synchronized as a stereo pair. A stereo pair of cameras with known parameters and relative pose allows estimation of 3D positions of points in space. The measurements were performed under natural sunlight conditions at 100-200 frames per second and a resolution of 800x600 pixels. A sequence of pictures of the desired events were captured from both cameras and converted to two videos, one for each camera. The videos were digitized using a free open source stereoscopy tracking software[14] and camera calibration data to perform 3D stereovision estimation of selected points on the target.

2. Data Postprocessing

Voids were left in the position series data for the tracked points due to body parts views obstructed by other body parts or by the environment. To fill these voids, a statistical software was used, applying a smoothing spline to the (x,y,z) data for each point over a flight. The lambda value for each spline was adjusted until a smooth curve was produced that followed the general path of the available points and bridged the voids in the data.

The tracked body part points were transformed into a fixed global coordinate system using tracked points on a reference target with a known position and orientation. After the points had been transformed into the global coordinate system, the pitch and yaw of the butterfly body vector(a vector from the abdomen root to the head) were calculated. These angles were used to define a butterfly body reference frame, a moving coordinate system with the origin at the abdomen root, the body vector pointing in the +X direction, the X-Z plane being the symmetry plane of the butterfly, with +Y facing left and +Z pointing up(with respect to the butterfly). The tracked points were transformed into the butterfly body frame so that the movement of the wingtips and abdomen with respect to the body could be analyzed.

III. Results

Simulation results for three motion input parameter sets were selected for display - 1) a random parameter set, 2) an optimized parameter set with fixed abdomen, and 3) an optimized parameter set with active abdomen actuation. Table 3 shows the motion parameters for the three sets. Table 4 displays characteristic flight parameters, including the Reynolds number(Re #) and the reduced frequency, k.[15,16]

Table 3. Motion parameter values for all simulations.

	φ (Flapping)			θ (Sweeping)			α (Feathering)			γ (Abdomen)			
Simulation	φ_A	φ_m	φ_p	θ_A	θ_m	θ_p	α_A	α_m	α_p	γ_A	γ_m	γ_p	f [Hz][a]
Random	48.9	-22.4	227.6	18.1	16.5	35.1	12.5	2.8	344.7	48.2	-20.5	349.4	9.79
Opt. #1[b]	52.4	23.0	8.9	7.9	-6.3	152.4	34.4	24.2	98.2	0	0	0	9.64
Opt. #2[c]	59.8	-25.1	127.6	12.5	-11.1	154.7	33.9	24.1	225.5	47.6	11.1	191.2	9.26

a Flapping and abdomen frequency
b Optimized parameters with fixed abdomen
c Optimized parameters with active abdomen actuation
* Subscripts A, m, and p indicate amplitude, mean, and phase, respectively
* All angles in degrees

A. Position and pitch histories

Figure 4 shows the position history for the three simulated flights over 20 flaps. Though the flights were optimized for 10 flaps, results were shown for 20 flaps as it takes time for the flight to reach a steady state,

Table 4. Flight characteristics for all parameter sets.

Flight	Re #	k
Random	4298	1.70
Opt. #1	4535	1.59
Opt. #2	4972	1.39

where the velocity and pitching velocity begin to repeat a pattern indefinitely. This steady state is the primary interest after the initial transient period has passed.

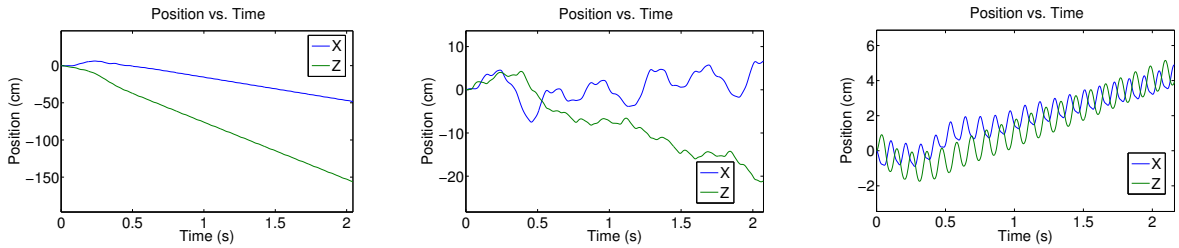

Figure 4. Time histories of position over 20 flaps for (a) random parameter set, (b) fixed-abdomen optimized parameter set, and (c) active-abdomen optimized parameter set.

For the random parameter solution, the butterfly begins descending rapidly and moves backwards. By $t = 0.5s$, it reaches steady state, where it moves backwards with a mean velocity of -31.3cm/s in the X-direction, with body position oscillations of amplitude 0.38cm. It descends with an average velocity of -76.9cm/s in the Z-direction, with oscillations of 0.56cm.

The fixed-abdomen solution reaches steady state shortly after $t = 0.5s$. The mean velocity in the X-direction is relatively small at 7.3cm/s, but has large body oscillations of 9.22cm. Though it initially ascends during the transient stage, at steady state the butterfly descends with an average velocity of -12.8cm/s in the Z-direction with 4.72cm oscillations.

The active-abdomen solution performs significantly better compared to the other solutions at steady state, achieving mean velocities of 2.1cm/s and 3.1cm/s in the X- and Z-directions, respectively, with body oscillations of 1.38cm and 1.65cm.

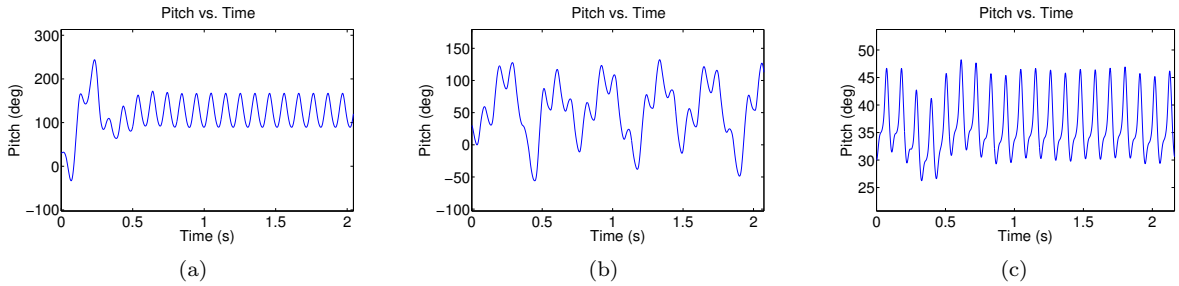

Figure 5. Time histories of pitch over 20 flaps for (a) random parameter set, (b) fixed-abdomen optimized parameter set, and (c) active-abdomen optimized parameter set.

Figure 5 shows the pitch histories for the three flights. The random solution reaches a steady state with a mean pitch of 124.3° with oscillations of 78.0°. For the fixed-abdomen solution, the steady state pitch has a mean of 50.0° and oscillates at a 180.9° amplitude. The active-abdomen solution, at steady state, has a mean pitch of 36.4° that oscillates at a 17.6° amplitude.

Observing the steady states, the active-abdomen solution clearly outperforms the others. In the X-direction, its average velocity is over 3x smaller than the fixed-abdomen solution, with oscillations in position

that are 6x smaller. In the Z-direction, its average velocity is over 4x smaller, with position oscillations almost 3x smaller. The active-abdomen solution performs even better with regards to the pitch history. The pitch oscillations of 17.9° are 10x smaller than the 180.9° amplitude of the fixed abdomen solution.

Though the random solution has smaller oscillations than the optimized solutions for the X- and Z-direction velocities, and smaller pitch oscillations than the fixed-abdomen solution, its significant mean velocities preclude hovering flight. With a mean pitch of 124.3°, almost upside-down, inverted flight is not a practical solution.

B. Forces and moments

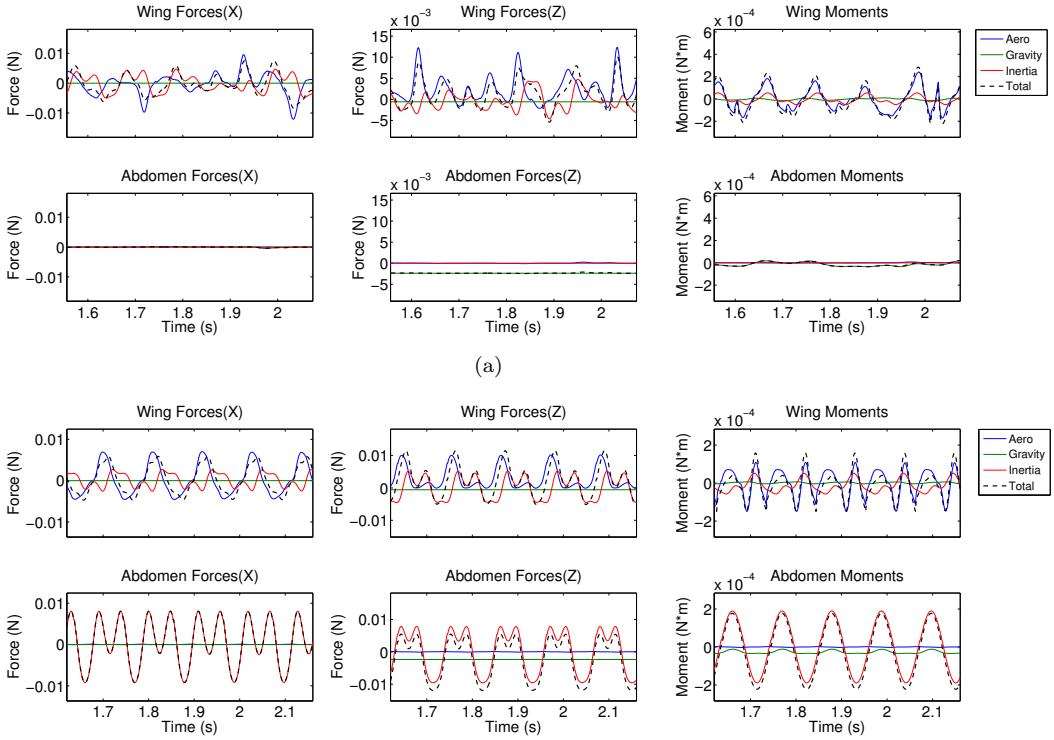

Figure 6. Force and moments due to aerodynamics, inertia, and gravity arising from the wings and abdomen over the last 5 flaps of the flight for (a) fixed-abdomen solution, and (b) active-abdomen solution.

To determine how the abdomen potentially enables the butterfly's increased stability in flight, the forces and moments from the wings and abdomen were examined for fixed-abdomen and active-abdomen flights, shown in Figure 6.

For the fixed-abdomen solution, the abdomen forces are small compared to the wing forces. There are no inertial forces as the abdomen is not accelerating relative to the body, and the abdomen drag is negligible compared to the wing aerodynamic forces. The moments arising from the abdomen forces are also relatively small - the only significant moment is due to the abdomen's gravity, which is still 5-10x smaller than the wing moments.

For the active-abdomen solution, significant forces arise in both the X- and Z-directions due to the abdomen inertia. These forces are on the same scale as the wing forces, however the abdomen inertia forces oscillate about zero, and therefore likely contribute little to the propulsion of the butterfly. These forces generate large moments that are on the same scale as the wing moments. It can also be observed that the two are in antiphase with each other, where the wing moments are at a maximum when the abdomen moments are at a minimum, greatly reducing the total moment on the butterfly, contributing to its stability. Such moments could also imply that the wings are given more freedom in their motion, and can focus on generating forces to propel the butterfly without being as tightly constrained by the moments they create.

C. Experimental flight data

A sample flight was selected for presentation that featured a long hovering sequence of a Tree Nymph. Figure 7 shows, for the sample flight, the wingtip motions in the X- and Z-directions of the body frame, as well as the abdomen tip motion in the Z-direction. The X- and Z-direction motion of the wingtips correlates to the sweeping and flapping angles of the wings, respectively, while the Z-direction motion of the abdomen correlates to its angle relative to the butterfly body. Examining the motion of these body parts with respect to each other gives insight into how they interact, and potentially how the butterfly stabilizes itself during hovering.

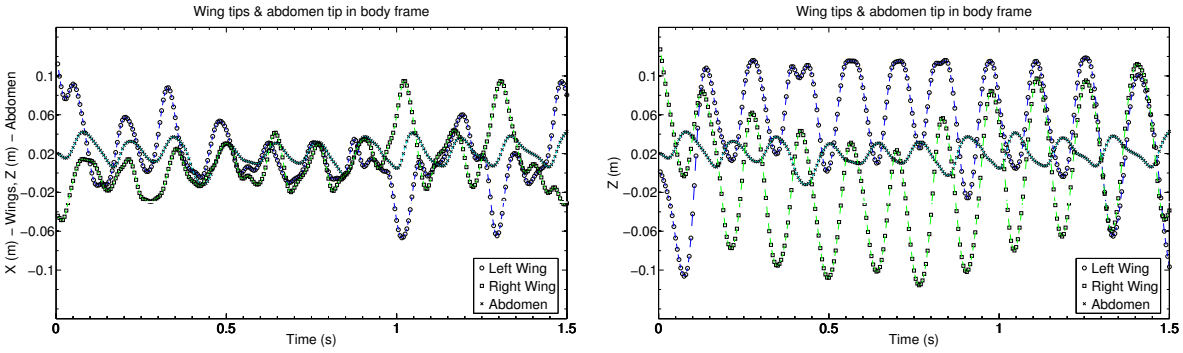

Figure 7. Wingtip motion in body frame in the (a) Z-direction and (b) X-direction, as well as the abdomen motion in the Z-direction for both plots.

In Figure 7(a), the wing sweeping and abdomen motion are in phase, with the wings moving forward as the abdomen moves down and vice versa. The sweeping of both wings is in phase for the majority of the flight, but two large out-of-phase strokes are seen near $t = 1s$ and $t = 1.25s$. The butterfly performs a yawing maneuver at this point of the flight, and may use out-of-phase sweeping strokes to execute the turns. The abdomen motion is consistent throughout the entire flight, even during the out-of-phase sweeping, and oscillates slightly above the body, with the tip staying above the X-axis of the body frame for most of the flight.

Figure 7(b) shows the flapping motion of the wings and the abdomen motion. The two are in anti-phase, with the abdomen moving upwards when the wings move downwards. The consistent oscillations of the abdomen in anti-phase with the wings could suggest the abdomen could possibly be used to dynamically balance the wing-flapping to stabilize the butterfly.

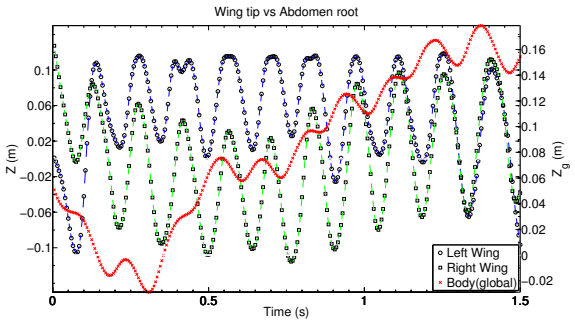

Figure 8. Wingtip motion in the Z-direction in the body frame with the abdomen root Z-position in the global frame.

Figure 8 displays the wing-flapping motion in the body frame with the abdomen root Z-direction position in the global frame. The abdomen root position oscillates slightly out-of-phase with the wings. As would be expected, the butterfly gains altitude during the downstroke of the wings, when the most downward force is generated, and falls during the upstroke.

IV. Conclusions

It is evident from the presented study that the motion of the abdomen plays a significant role in the stabilization of the butterfly in hovering. At steady state, the optimized active-abdomen parameter set outperformed its fixed-abdomen counterpart. A smaller average velocity in both forward and vertical directions was observed for the active-abdomen solution, and the amplitude of its position oscillations were also significantly less. The active-abdomen solution was also significantly more stable in pitch, with oscillations of roughly 20°, compared to the 180° oscillations of the fixed-abdomen solution. Reduced oscillations in velocity and pitch could provide relevant advantages for vision-based flight control, typical of insects.

The forces and moments during the two optimized flights gave insight into the abdomen motion function in stabilizing the butterfly. As the abdomen moments were capable of countering the wing moments to reduce the total pitching moment, pitching stability was greatly increased. The ability of the abdomen to generate large pitching moments could also potentially give the butterflies considerable freedom, allowing them to focus on wing motion that generates desired forces for propulsion, without having to fully account for the inertial moments generated. Though the abdomen actuation generated significant forces, these forces oscillated about a mean of roughly zero, and therefore did not appear to contribute to the propulsion of the butterfly.

Examination of experimental data from a recorded butterfly flight showed large abdomen movements that were in anti-phase with the wing-flapping motion, confirming that the abdomen may be used to dynamically balance the wing-flapping to provide stability during hovering. When examining the abdomen root position in the Z-direction with the wing-flapping motion, it appears that the butterfly gains altitude during the downstroke of the wings and subsequently loses altitude during the upstroke, as would be expected. This oscillating force allows the butterfly to maintain close to a fixed position in hovering.

V. Acknowledgements

The authors would like to acknowledge the past support from the Air Force Research Laboratory, Munitions Directory at Elgin AFB, FL, as well as the support of Oregon State University. The authors would also like to thank the McGuire Center for Lepidoptera & Biodiversity for allowing the gathering of data necessary for this project and other related projects, as well as their continuous care and support of the butterflies residing there. Finally, a special thanks to Dr. Ty Hedrick, who provided the code for his hawkmoth model, which was used as a foundation for the butterfly model outlined in this paper.

References

[1]Lindhe Norberg, U. and Winter, Y., "Wing beat kinematics of a nectar-feeding bat, *Glossophaga soricina*, flying at different flight speeds and Strouhal numbers," *The Journal of Experimental Biology*, Vol. 209, 2006, pp. 3887–3897.

[2]Tobalske, B., Warrick, D., Clark, C., and Powers, D., "Three-dimensional kinematics of hummingbird flight," *The Journal of Experimental Biology*, Vol. 210, 2007, pp. 2368–2382.

[3]Liu, Y. and Sun, M., "Wing kinematics measurement and aerodynamics of hovering droneflies," *The Journal of Experimental Biology*, Vol. 211, 2008, pp. 2014–2025.

[4]Chakravarthy, A., Albertani, R., and Evers, J., "In-Flight Dynamically Adaptive Configurations: Lessons from Live Lepidoptera," *18th AIAA/ASME/AHS Adaptive Structures Conference*, Orlando, FL, April 2010.

[5]Wang, J. and Sun, M., "A computational study of the aerodynamics and forewing-hindwing interaction of a model dragonfly in forward flight," *The Journal of Experimental Biology*, Vol. 208, 2005, pp. 3785–3804.

[6]Hedrick, T. L. and Daniel, T. L., "Flight control in the hawkmoth *Manduca sexta*: the inverse problem of hovering," *The Journal of Experimental Biology*, Vol. 209, 2006, pp. 3114–3130.

[7]Dickinson, M., Lehmann, F., and Sane, S., "Wing Rotation and the Aerodynamic Basis of Insect Flight," *Science*, Vol. 284, 1999, pp. 1954–1960.

[8]Usherwood, J. and Ellington, C., "The aerodynamics of revolving wings," *The Journal of Experimental Biology*, Vol. 205, 2002, pp. 1547–1564.

[9]Sane, S., "The aerodynamics of insect flight," *The Journal of Experimental Biology*, Vol. 206, 2003, pp. 4191–4208.

[10]Sane, S. and Dickinson, M., "The aerodynamic effects of wing rotation and a revised quasi-steady model of flapping flight," *The Journal of Experimental Biology*, Vol. 205, 2002, pp. 1087–1096.

[11]von Mises, R., *Theory of Flight*, Dover, 1959.

[12]Kundu, P., *Fluid Mechanics*, Academic Press, 1990.

[13]Albertani, R., Goettl, M., and Wilson, T., "A Wind Tunnel Investigation of *Lepidopterae* Flight in Cross-Wind Conditions," *51st AIAA Aerospace Sciences Meeting*, 2013.

[14]Hedrick, T. L., "Software techniques for two and three-dimensional kinematic measurements of biological and biomimetic systems," *Journal of Bioinspiration and Biomimetics*, Vol. 3, 2008, pp. 034001.

[15]Dickson, W. and Dickinson, M., "The effect of advance ratio on the aerodynamics of revolving wings," *The Journal of Experimental Biology*, Vol. 207, 2004, pp. 4269–4281.

[16]Shyy, W., Aono, H., Chimakurthi, S., and Trizila, P., "Recent progress in flapping wing aerodynamics and aeroelasticity," *Progress in Aerospace Sciences*, Vol. 46, 2010, pp. 284–327.